coatings

Article

Study on Microstructure and Properties of Additive-Manufactured TC4ELI+TC21 Titanium Alloy Gradient Composite Structures

Can Cui [1], Haibin Ji [2], Sensen Han [2,3,*], Minghao Xuan [1], Bin Wu [1], Pengxu Li [4] and Qingshi Meng [1,3,*]

1 Shenyang Aircraft Design Institute, Shenyang 110001, China; cuican1978@163.com (C.C.)
2 Shi-Changxu Innovation Center for Advanced Materials, Institute of Metal Research, Chinese Academy of Sciences, Shenyang 110016, China
3 College of Aerospace Engineering, Shenyang Aerospace University, Shenyang 110136, China
4 National Engineering Research Center of Near-Net-Shape Forming for Metallic Materials, South China University of Technology, Guangzhou 510640, China
* Correspondence: sauhansen@163.com (S.H.); mengqingshi@hotmail.com (Q.M.)

Abstract: TC4ELI+TC21 titanium gradient composite structures with direct transition (TD1) and cross transition (TD2) were prepared using laser deposition manufacturing technology. The microstructure of the gradient interface was observed, and the distribution of alloying elements was detected. The tensile properties of the two alloys at room temperature were tested, and the effects of different heat treatment regimens on the microstructure and mechanical properties were investigated. The results show that there is no obvious defect at the gradient interface of the two alloys. Compared with direct transition alloys, the alloying elements of TD2 alloys change less at the interface, the structure of the transition zone is more closely bound, and the elongation is higher. After heat treatment, the α phase in the alloy is coarsened, and the alloy elements at the interface are fully diffused, so that the gradient interface of the alloy is eliminated to a certain extent, the tensile strength of the alloy decreases, and elongation increases. The strength and plasticity of the alloy reached their best match at a solution temperature of 930 °C.

Keywords: gradient composite structures; titanium alloy; laser deposition manufacturing; heat treatment; mechanical property

Citation: Cui, C.; Ji, H.; Han, S.; Xuan, M.; Wu, B.; Li, P.; Meng, Q. Study on Microstructure and Properties of Additive-Manufactured TC4ELI+TC21 Titanium Alloy Gradient Composite Structures. *Coatings* **2024**, *14*, 104. https://doi.org/10.3390/coatings14010104

Academic Editor: Hideyuki Murakami

Received: 26 October 2023
Revised: 29 November 2023
Accepted: 4 December 2023
Published: 12 January 2024

1. Introduction

Conventional structural components are typically made of homogeneous materials that exhibit singular and uniform properties. Metal gradient composite structures combine two or more metallic materials into a single entity, resulting in a gradient variation of mechanical properties [1,2]. With the continuous development of the aerospace industry, components are constantly evolving towards integration and functional structuration, presenting a clear demand for dual-performance composites in which different parts of the integral components possess distinct properties [3]. As a typical non-uniform structure, the gradient composite structure has good designability and can optimize material layout according to the performance requirements of the component. By changing the composition and microstructure of the gradient composite structure, it is possible to achieve different functions in different regions. These characteristics, which traditional materials cannot match, make gradient composite structures promising prospects for development and applications in aerospace and other fields. However, such structures are usually difficult to achieve through traditional casting or forging methods.

At present, there are many preparation methods for Functionally Graded Materials (FGMs); commonly used methods include additive manufacturing (AM) processes (i.e., selective laser melting, laser deposition manufacturing, wire arc AM, etc.), plasma spraying, powder metallurgy, etc. [2,4–6]. Among these, laser deposition manufacturing (LDM) technology is a manufacturing technology developed on the basis of rapid prototyping and laser cladding technology [7,8]. It is an ideal method for preparing gradient composite structures. The technology uses a coaxial real-time variable ratio powder-feeding method in which metal powder is melted with a high-power laser beam, and gradient distribution of materials and properties is achieved through layer-by-layer stacking. This technology can conveniently and quickly manufacture large-sized, complex-shaped, and high-performance gradient structures [9]. Titanium alloys are widely used in the aerospace field due to their good corrosion resistance, low density, high specific strength, and toughness [2,10,11]. In recent years, many scholars have conducted extensive research on the material design, preparation, and performance analysis of titanium alloy gradient structures due to their considerable potential for application.

Lei et al. [12] used laser metal deposition to prepare gradient materials of Ti6Al4V and SS316. They found that when stainless steel metal powder was directly deposited on a titanium alloy substrate, the hard and brittle Fe-Ti intermetallic compound generated at the interface caused direct cracking of the sample at the interface under thermal stress. Abioye et al. [13] used laser metal deposition technology to simultaneously feed Ni powder and commercially pure titanium to prepare Ti-Ni gradient layers with continuously varying composition. The microstructure, phase composition, and microhardness were analyzed. He Bo et al. [2] prepared TA15/TiAlNb composite structures using synchronous powder-feeding LDM technology followed by different heat treatments. The results showed that the microstructure transition interface of the gradient composite sample with a three-layer transition layer exhibited no obvious defects and that the fractures of as-deposited samples have more characteristics of cleavage fracture, while the fractures of heat-treated samples show a ductile feature.

TC4 and TC21 titanium alloys are both $\alpha + \beta$ dual-phase titanium alloys. TC4 titanium alloy can work for a long time at temperatures up to 400 °C and has excellent comprehensive properties. It is mainly used in the manufacture of aircraft structures and aerospace engine blades and is the most widely used medium-strength titanium alloy [14,15]. Low-interstitial TC4 (TC4ELI) is a damage-tolerant titanium alloy based on TC4 titanium alloy, which is developed by optimizing and adjusting the alloy elements. It has high fracture toughness and a low crack propagation rate. TC21 titanium alloy is a new type of high-strength, high-toughness, and damage-tolerant titanium alloy. Due to its excellent strength, plasticity, and fracture toughness, it has attracted more and more attention in the past decade [11,16]. Integrating a high-damage-tolerant TC4ELI titanium alloy with a high-strength TC21 titanium alloy can achieve a combination of strength and toughness on the same component, enabling the performance advantages of each material to be fully utilized and improving structural efficiency. The combination of high-damage-tolerant TC4ELI titanium alloy and high-strength TC21 titanium alloy on the same component can realize a combination of strength and toughness, make full use of the performance advantages of each material, and improve the service efficiency of the structural components. Currently, there is limited research on additive manufacturing and LDM of TC4ELI+TC21 titanium alloy gradient composite structures. In this study, TC4ELI+TC21 titanium alloy gradient composite structures with two different transition modes were fabricated using LDM technology with TC4ELI and TC21 titanium alloy powders as raw materials. The microstructure was observed, and tensile properties were tested at room temperature to investigate the effect of transition mode on the bonding quality of the gradient interface with the goal of providing technical support for the application of TC4ELI+TC21 titanium alloy gradient composite structures in the aerospace field.

2. Experiment

2.1. Materials

The TC4ELI and TC21 titanium alloy powders used in this paper, with an average size of 75–185 μm, as shown in Figure 1, were prepared using the gas atomization method

(Bright Laser Technologies Co., Ltd., Xi'an, China). The chemical compositions are shown in Table 1.

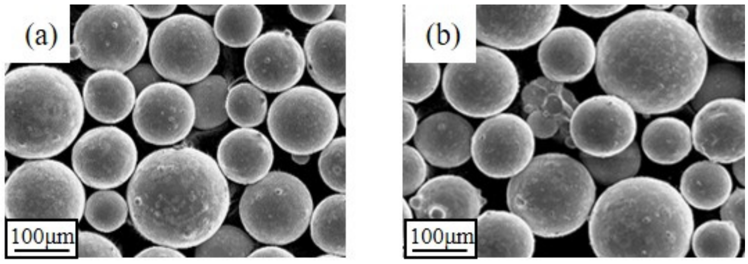

Figure 1. Scanning electron microscope (SEM) images of (**a**) TC4ELI and (**b**) TC21 powder.

Table 1. Chemical composition of TC4ELI and TC21 titanium alloy powders (wt.%).

Element	Al	V	Zr	Sn	Mo	Gr	Nb	N	H	O	Ti
TC4ELI	6.00	4.07	-	-	-	-	-	0.0082	<0.002	0.086	Bal.
TC21	6.48	-	1.96	2.07	2.99	1.47	2.04	0.0036	<0.002	0.10	Bal.

2.2. Preparation

Laser coaxial powder-feeding LDM-forming equipment (BLT-C600, Bright Laser Technologies Co., Ltd., Xi'an, China) was used to fabricate two TC4ELI+TC21 titanium alloy gradient composite structures with direct and cross transitions (TD1, TD2) in the manner illustrated in the forming diagram shown in Figure 2. Firstly, the sample model was sliced and layered with a certain thickness using slicing software (BLT-Build Planner, Xi'an, China), converting the three-dimensional shape information of the sample into two-dimensional contour information, and generating a scan trajectory file. Then, under the control of a numerical control system, the TC4ELI and TC21 titanium alloy powders were melted and stacked layer by layer by coaxial powder feeding, using a laser as a heat source. The optimized working parameters used in this study are listed in Table 2.

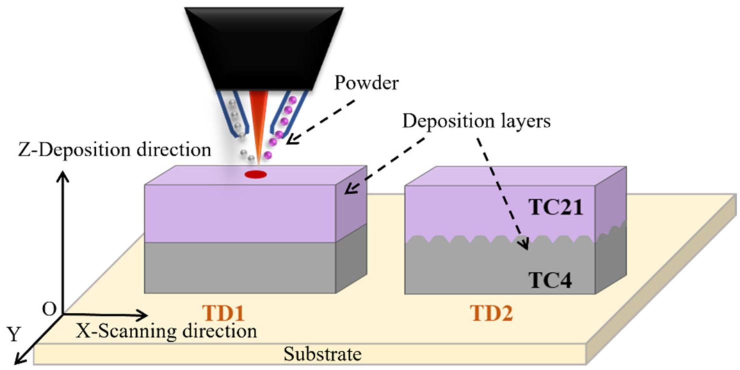

Figure 2. Schematic diagram of TC4ELI+TC21 titanium alloy gradient composite structures forming sample.

Table 2. Optimized LDM working parameters used in this study.

LDM Conditions	Parameters
Laser power	1700 W
Scanning speed	800 mm/min
Spot diameter	4 mm
Powder-feeding rate	13.3 g/min
Layer thickness	0.45 mm

2.3. Characterization

To investigate the effect of heat treatment on the microstructure of as-deposited TC4ELI+TC21 titanium alloy gradient composite structures, a solution aging process was used to heat treat the as-deposited TC4ELI+TC21 titanium alloy sample according to the heat treatment parameters shown in Table 3. Metallographic samples were obtained by wire cutting from the LDM samples (the observation surface was XOZ, as shown in the coordinate system in Figure 1), with the cutting plane extending 10 mm on both sides of the interface in the direction perpendicular to the interface and 20 mm in the direction parallel to the interface, resulting in metallographic samples with an area of 20 mm × 20 mm.

Table 3. Heat treatment system of TC4ELI+TC21 titanium alloy gradient composite structures.

Sample	Heat Treatment
TD1	900 °C × 2 h/AC + 500 °C × 5 h/AC
	930 °C × 2 h/AC + 500 °C × 5 h/AC
	960 °C × 2 h/AC + 500 °C × 5 h/AC
TD2	900 °C × 2 h/AC + 500 °C × 5 h/AC
	930 °C × 2 h/AC + 500 °C × 5 h/AC
	960 °C × 2 h/AC + 500 °C × 5 h/AC

The samples were first mechanically polished and then etched with a corrosive liquid (HNO_3:HF:H_2O = 1:1:3 by volume). The microstructure was observed using optical microscopy (OM, Zeiss Ax overt 200MAT, Oberkochen, Germany) and a field emission scanning electron microscope (SEM, Hitachi SU-70, Tokyo, Japan) coupled with EDS. The phase composition was examined using X-ray diffraction (XRD, D/MAX, Japan).

Mechanical property test samples were cut parallel to the deposition direction and the axis of the tensile bar. The interfaces of the TD1 and TD2 alloy samples were located in the center of and perpendicular to the direction of the tensile load. The rod-like mechanical property test samples were sampled along the *Z*-axis by wire cutting from LDM samples. Note that the material interface of TD1 and TD2 alloy specimens was located at the center line of the tensile sample, perpendicular to the direction of tensile load. A universal testing machine (TSE504D, Wance Technologies Co., Ltd., Shenzhen, China) was used to test the tensile mechanical properties of the samples at room temperature in accordance with the requirements of the GB/T 228.1-2010 [17] tensile testing standard for metallic materials.

3. Results and Discussion

3.1. Microstructure and Composition Evolution

Figure 3 presents the XRD patterns of the LDM samples before and after heat treatment. Both TC4ELI and TC21 samples have an α/α' diffraction peak, and the α and α' phases have similar lattice parameters in a close hexagonal packed structure, so the XRD patterns are difficult to tell apart. A small number of β phase diffraction peaks also appear in the formation of TC21, which indicates that more β stable elements can retain β phase at room temperature during the laser additive manufacturing forming process.

Figure 4a,b show the longitudinal section obtained by optical microscopy (OM) and SEM microstructure of the as-deposited TD1 alloy, respectively. Figure 4c,d, respectively, show the longitudinal sections obtained by optical microscopy (OM) and SEM microstructures of the as-deposited TD2 alloy. Coarse columnar β grains can be observed in pure TC4ELI and TC21 titanium alloy. During the LDM process, a preferred crystal orientation along the deposition direction gradually formed, with the growth direction perpendicular to the substrate. This is because, during the forming process, the temperature gradually increases from the bottom to the top of the melt pool, and most of the heat loss occurs along the deposition direction and perpendicular to the substrate, resulting in a higher temperature gradient along the deposition direction [7]. At the same time, the solidification of the melt pool starts from the bottom, and the solidification rate gradually increases, which leads to the formation of columnar grains. The melt pool formed by the next layer causes partial remelting of the previous layer's columnar grains, resulting in continuous epitaxial growth of the original β columnar grains along the deposition direction. There is a large amount of α phase inside the columnar grains; this is because, during the deposition process, the α phase nucleates and grows at the grain boundaries or within the grains. The α phases grow in different directions and at different speeds and stop growing after contacting each other, resulting in fast-growing α phase-forming plate-like or needle-like shapes and slow-growing α phase-forming, short, rod-like shapes [18].

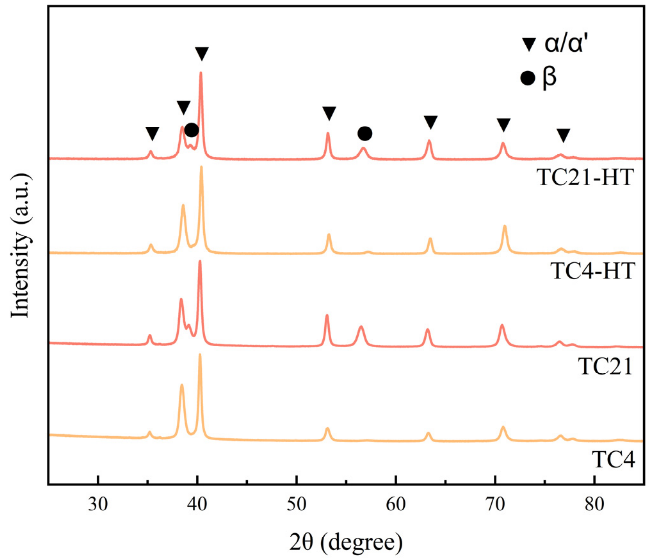

Figure 3. The XRD patterns of TC4ELI and TC21 alloys as-deposited and after heat treatment.

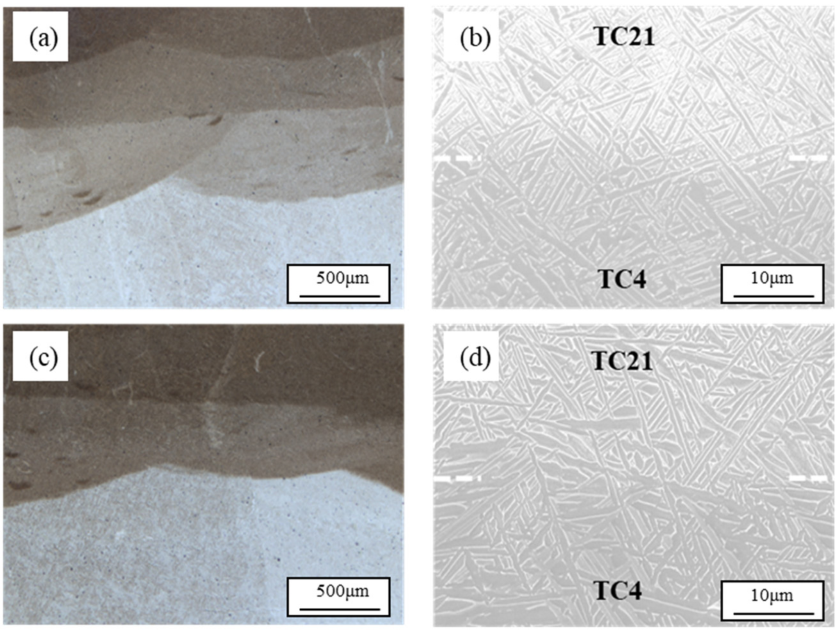

Figure 4. OM and SEM microstructure of as-deposited alloys: (**a**,**b**) TD1 and (**c**,**d**) TD2.

Elemental analysis of the gradient interface region of as-deposited TD1 and TD2 alloys was performed using an energy-dispersive X-ray spectroscopy (EDS) analyzer. Figure 5a,b show the line scan results of the gradient interfaces of TD1 and TD2 alloys. The main elements Ti, Al, V, Zr, Sn, Mo, Nb, and Cr diffused sufficiently at the interface, and the gradient interface region of the alloying element content showed certain regularity from the TC4ELI titanium alloy region to the TC21 titanium alloy region, as shown in line scan results. The contents of Ti and V gradually decreased, while the contents of Zr, Sn, Mo, and Nb gradually increased, and a certain degree of mutation occurred at the gradient interface. However, the distribution of Al and Cr at the gradient interface between TD2 and TD1 alloys was relatively uniform due to the small concentration gradient. Compared to the TD2 alloy, the TD1 alloy had a greater degree of mutation in the interface elements, as shown in Figure 5a, which may be due to the slower cooling rate of the interface during the cooling process of the cross transition.

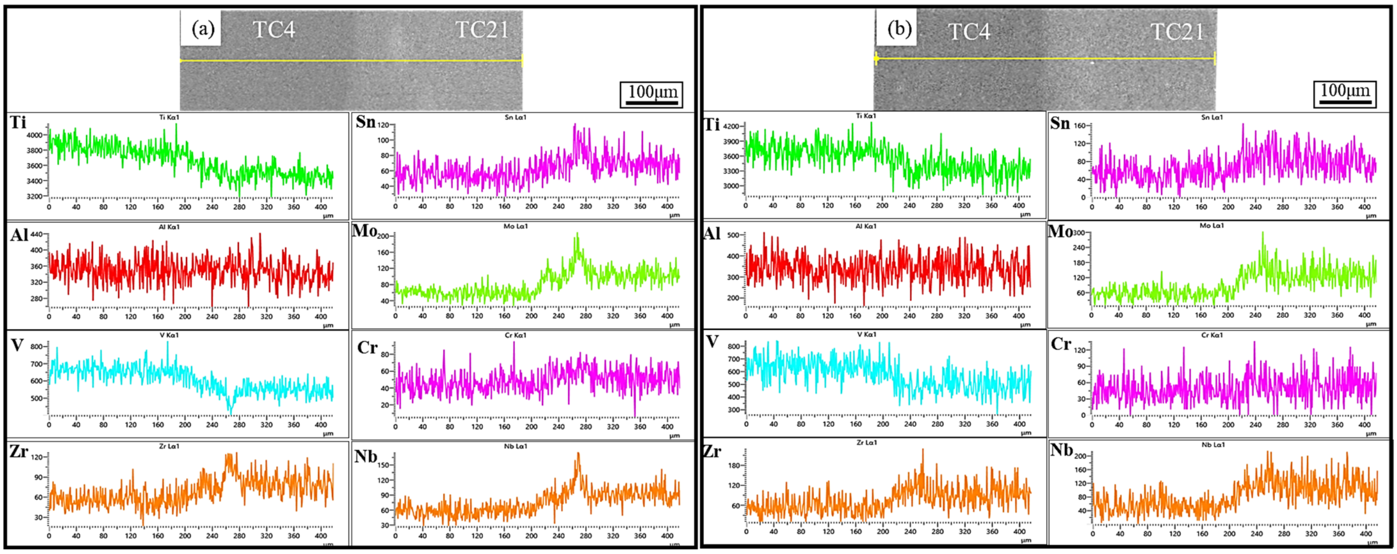

Figure 5. EDS line sweep results at the interface of as-deposited alloy (**a**) TD1 and (**b**) TD2.

To analyze the elemental changes at the gradient interface more accurately, the interface region was tested using the EDS surface scanning method, as shown in Figure 6. As can be seen in Figure 6a,b, the distributions of alloying elements Zr, Sn, Mo, and Nb obviously differ across the interface, resulting in a clear boundary line that was consistent with the distribution pattern of elements shown in Figure 5.

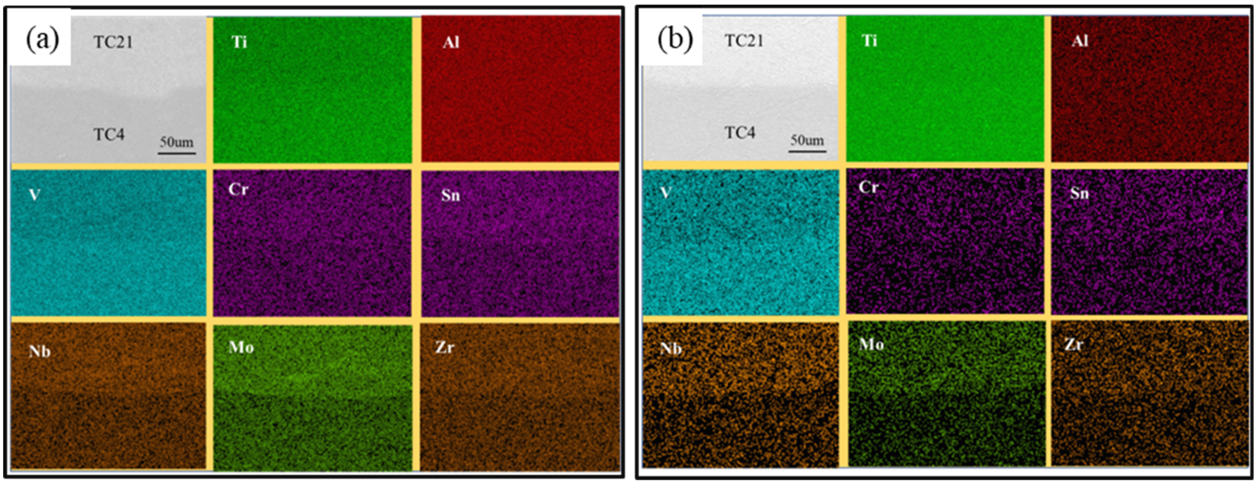

Figure 6. EDS surface scan results at the interface of as-deposited alloys (**a**) TD1 and (**b**) TD2.

Figures 7 and 8 show the microstructures of TD1 and TD2 alloys at different solution temperatures. It can be seen that the microstructure of the TC4ELI titanium alloy region of the alloy has changed significantly. After heat treatment, the α-platelets coarsen significantly, and the coarsening phenomenon becomes more apparent with increasing solution temperature. When the solution temperature is 960 °C, a large number of short rod-shaped α-phase appear, and the α-phase exhibits characteristics of spherodization, as shown in Figures 7c and 8c. In the TC21 titanium alloy region, after heat treatment at 900 °C, the needle-like α-phase in the forming state gradually transforms into coarse α-platelets through nucleation and growth processes [19], as shown in Figures 7a and 8a.

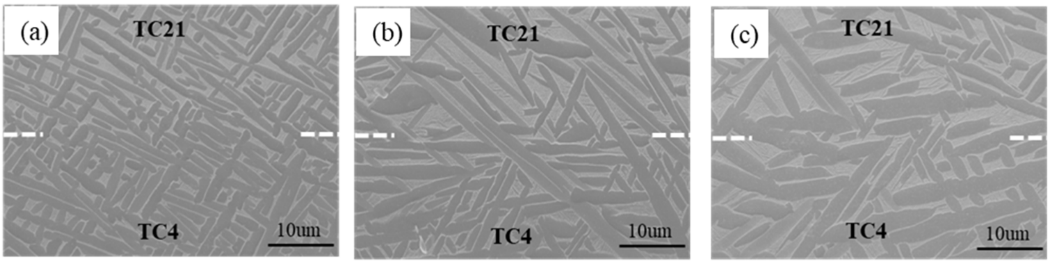

Figure 7. Microstructure of the TD1 alloy at different heat treatment temperatures: (**a**) 900 °C, (**b**) 930 °C, and (**c**) 960 °C.

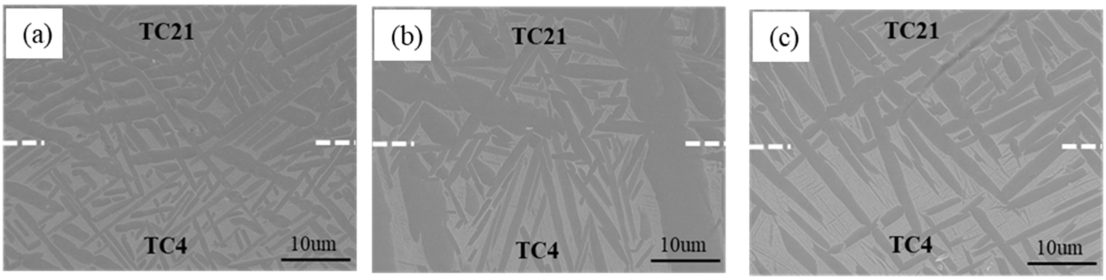

Figure 8. Microstructure of TD2 alloy at different heat treatment temperatures: (**a**) 900 °C, (**b**) 930 °C, and (**c**) 960 °C.

In the process of heat treatment at lower temperatures, a large number of small needle-like α-phase formed during the LDM process may become nucleation particles for α-platelets and directly transform into plate-like α-phase through diffusion phase transformation [20]. Therefore, the size of the α-phase significantly increases after heat treatment; as the heat treatment temperature gradually increases to 960 °C, close to the phase transition point of the TC21 titanium alloy, some of the plate-like α-phase transformed from the needle-like α-phase converts to β-phase through element diffusion. With the increase in heat treatment temperature, the volume fraction of β-phase gradually increases, and the β-phase with a certain orientation merges and grows. During the cooling process, the β-phase nucleates and transforms into α-phase at the two-phase interface, promoting the growth of α-phase, and thus the size of the plate-like α-phase gradually coarsens [20], as shown in Figures 7c and 8c.

After heat treatment, the gradient interface between the TC4ELI titanium alloy and the TC21 titanium alloy in TD-1 and TD2 alloys is not clear. On the one hand, this is because of the decomposition and regeneration of phases at the gradient interface at high temperatures. Figure 9a,b show the results of the line scan centered on the gradient interface of heat-treated TD1 and TD2 alloys; comparing these with the results in Figure 5, it can be seen that the mass fractions of Ti, Al, V, Cr, Sn, Nb, Mo, and Zr alloy elements in the TC4ELI titanium alloy and TC21 titanium alloy regions are almost the same, indicating that the alloy elements have undergone sufficient diffusion during the heat treatment process, promoting the decomposition and regeneration of phases at the interface and, to some extent, eliminating the gradient interface of the alloy. On the other hand, the structure at the interface gradually coarsens at high temperatures. The coarsened α-platelets in the TC4ELI titanium alloy region at the interface and the β-phase in the TC21 alloy region combine and grow together, resulting in greater blurring of the gradient interface, as shown in Figures 7 and 8.

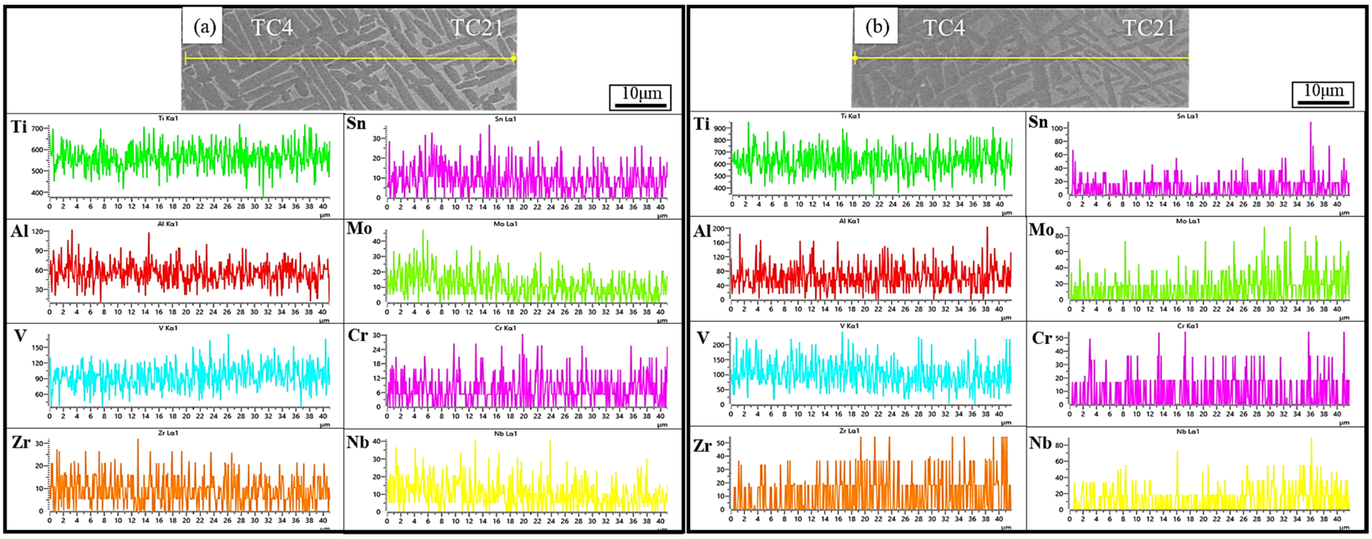

Figure 9. EDS line sweep test results at the alloy interface after heat treatment at 930 °C: (**a**) TD1 and (**b**) TD2.

3.2. Mechanical Properties and Fracture Behaviour

Figure 10a,b present the room-temperature tensile properties of TD1 and TD2 alloys before and after heat treatment. From the graphs, it can be seen that the changes in the tensile properties of the alloy with gradient interface transition mode were consistent after heat treatment, with a decrease in tensile strength and an increase in elongation. After solution treatment at 900 °C, the tensile strengths of TD1 and TD2 alloys were 888 Mpa and 890 Mpa, respectively, which decreased by 52 Mpa and 44 Mpa compared to the as-deposited samples (with tensile strengths of 940 Mpa and 934 Mpa), representing decrease rates of 5.5% and 4.7%, respectively. After solution treatment at 960 °C, the tensile strengths of the two alloys were 881 Mpa and 877 Mpa, respectively, which were not significantly different from those after solution treatment at 900 °C and 930 °C. The elastic modulus of the TD1 alloy increased first and then decreased with the increase in heat treatment temperature, and the lowest was 111 Gpa, which was lower than that of the deposited alloy. However, the TD2 alloy showed a different trend, and the elastic modulus decreased with the increase in heat treatment temperature; the lowest value was 119 Gpa. The elongation of the TD1 alloy reached its highest value of 13% after heat treatment at 900 °C, which increased by 56.6% compared to the as-deposited state of 8.3%. The elongation of the TD2 alloy reached its highest value of 14.7% after heat treatment at 900 °C, which increased by 36% compared to the as-deposited state of 10.8%. After heat treatment, the strength of the alloy decreased, and the plasticity improved primarily due to the spheroidization of the α-platelets in the TC4ELI titanium alloy region and the transformation of the needle-like α-phase in the TC21 titanium alloy region into α + β phase as shown in Figures 7 and 8 [21]. Secondly, after heat treatment, the α-phase clearly coarsened, and the β-phase content increased significantly. The strength of the β-phase is lower than that of the α-phase, but its plasticity is higher than that of the α-phase, which ultimately leads to a decrease in strength and an increase in plasticity of the samples after heat treatment. However, when the heat treatment temperature was increased from 930 °C to 960 °C, the plasticity of the samples did not improve; this is because the alloy was close to the phase transition point of TC21, the proportion of composition phases in the alloy changed, and the degree of coarsening increased as shown in Figures 7c and 8c, producing significant dislocation stress, which led to a decrease in plasticity [22]. Therefore, the tensile strength and plasticity of the TD1 and TD2 alloys were optimally matched at solution temperatures of 900 °C and 930 °C, respectively.

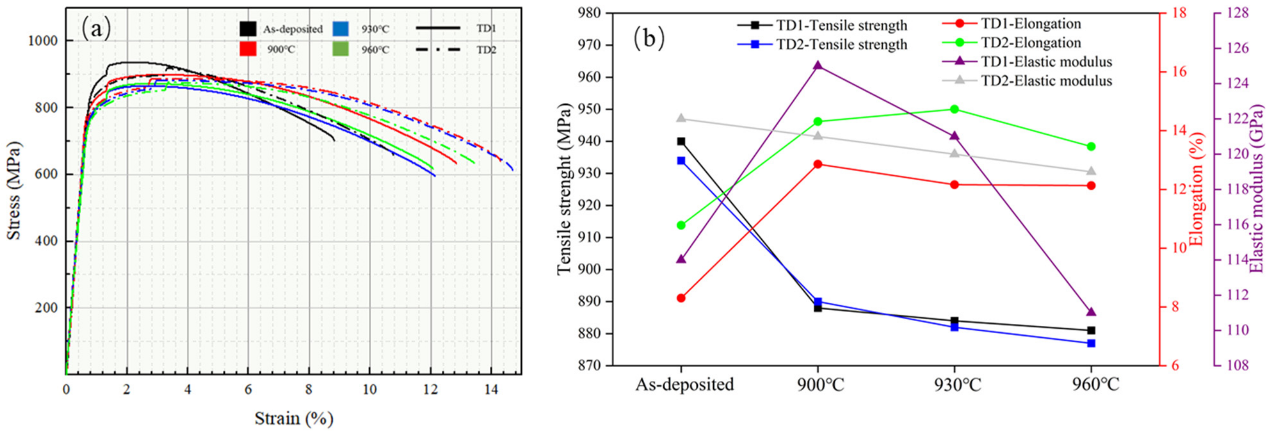

Figure 10. (**a**) Stress–strain curves and (**b**) tensile properties of TD1 and TD2 alloys under different heat treatment.

As shown in Figure 10b, the maximum difference in tensile strength between the TD1 and TD2 alloys in each state was 6 MPa (as-deposited), which is only 0.6% of that of the TD1 alloy. However, in terms of elongation, compared with the TD1 alloy, the TD2 alloy showed an upward trend in all states, and the difference in elongation at 900 °C heat treatment was the largest, reaching 4.5%. The higher plasticity of the TD2 alloy is due to the fact that the composition of the TC4ELI titanium alloy region and the TC21 titanium alloy region at the gradient interface of the TD2 alloy were mutually interlocked and grown together, resulting in a more compact microstructure. In addition, it can be seen from Figure 10b that the fracture position of the room-temperature tensile samples of the TD1 and TD2 alloys in the as-deposited and heat-treated states was close to the shoulder of the samples and that no fracture occurs at the gradient interface, indicating that the combined quality of the two transition modes of the alloy resulted in no obvious defects at the gradient interface during the LDM process.

Figure 11 shows the SEM fracture morphology of the room-temperature tensile samples of the TD1 and TD2 gradient composite structures to further investigate the effect of heat treatment on the mechanical properties of the material. Figure 11a (TD1) and Figure 10b (TD2) show the macroscopic fracture morphology in the as-deposited state. The fracture surface of the alloy sample is a cup-and-cone fracture, with obvious shear lips and instantaneous fracture zones at the periphery of the fracture. The center of the fracture is the fiber region. Figure 11e,f show the local magnification of the center of the fracture in Figure 11a,b; shallow dimples and tear edges are present on the fracture surface, and obvious cleavage planes appear in some areas. It is believed that there are many relatively small α-phase layers in the as-deposited sample (Figure 4), which result in a large number of phase boundaries inside the alloy. Dislocations accumulate at the phase boundaries to form stress concentration zones. Therefore, microcracks form and propagate at the phase boundaries under tensile stress, resulting in poor plasticity. Figure 11c,d show the macroscopic fracture morphology of the TD1 and TD2 alloys at a solution temperature of 930 °C. It can be observed that the fracture surfaces of the alloys show obvious plastic deformation with mixed fracture characteristics. The center of the fracture is the fiber region, which is surrounded by shear lips and tear edges. The surface shows uneven, shallow dimples and pores. The position of the crack source is located in the fiber region. The fracture process entails pore nucleation, growth, and fusion, which is a typical ductile fracture with dimple aggregation. Compared with the as-deposited sample, the proportion of fiber region after treatment is larger and the dimples are deeper, which is because the α-platelets become wider and tend to be spheroidized after heat treatment (as shown in Figures 7 and 8), leading to an increase in slip distance and plasticity and a decrease in strength [23,24]. The fracture morphology characteristics observed on the fracture surfaces of the alloy samples are consistent with the mechanical property test results shown in Figure 9.

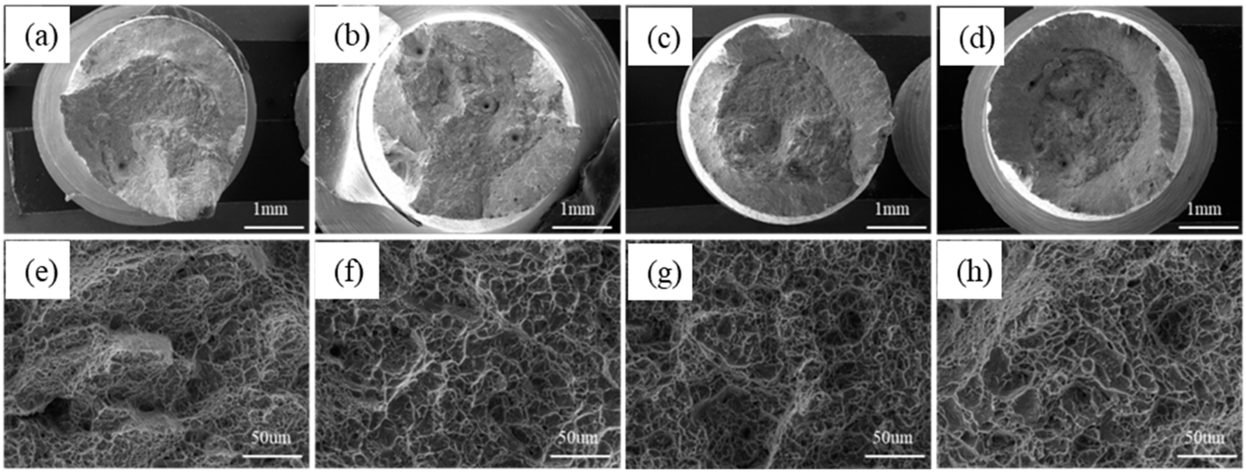

Figure 11. Fracture morphology of alloy tensile specimens: (**a**,**e**) TD1: as-deposited, (**b**,**f**) TD2: as-deposited, (**c**,**g**) TD1-930 °C: heat-treated, and (**d**,**h**) TD2-930 °C: heat-treated.

4. Conclusions

In summary, using LDM technology, two titanium alloy (TC4ELI+TC21) gradient composite structure samples of direct transition (TD1) and cross transition (TD2) were prepared, and the influence mechanism of the heat treatment process on their properties was investigated. The interface region of the gradient composite structures exhibited no obvious defects and displayed good quality. There was a certain degree of elemental composition change at the gradient interface. In comparison with the TD1 alloy, the interface of the TD2 alloy was less pronounced, and the degree of variation of alloy elements at the interface was smaller. The transition zone exhibited a more compact structure, resulting in greater elongation, although there was little difference in tensile strength between the two samples. Following heat treatment, the small α-phase of the alloy coarsened, and alloying elements at the interface fully diffused, leading to a decrease in tensile strength and an increase in elongation. The strength and plasticity of the TD1 and TD2 alloys were optimally matched at solution temperatures of 900 °C and 930 °C, respectively. This research lays the foundation for additive manufacturing of heterogeneous gradient composite structures.

Author Contributions: Methodology, H.J., S.H., M.X. and B.W.; Validation, H.J. and B.W.; Formal analysis, C.C., H.J., S.H., M.X. and P.L.; Investigation, C.C. and S.H.; Data curation, C.C., M.X., B.W., P.L. and Q.M.; Writing—original draft, C.C., H.J. and B.W.; Writing—review & editing, C.C., H.J., S.H., M.X., P.L. and Q.M. All authors have read and agreed to the published version of the manuscript.

Funding: This research received no external funding.

Institutional Review Board Statement: Not applicable.

Informed Consent Statement: Not applicable.

Data Availability Statement: Data are contained within the article.

Conflicts of Interest: The authors declare no conflict of interest.

References

1. Su, Y.; Chen, B.; Tan, C.; Song, X.; Feng, J. Influence of composition gradient variation on the microstructure and mechanical properties of 316 L/Inconel718 functionally graded material fabricated by laser additive manufacturing. *J. Mater. Process. Technol.* **2020**, *283*, 116702. [CrossRef]
2. He, B.; Wu, D.; Pan, J.; Yang, G. Effect of heat treatment on microstructure and mechanical properties of laser deposited TA15/Ti_2AlNb gradient composite structures. *Vacuum* **2021**, *190*, 110309. [CrossRef]
3. Reichardt, A.; Shapiro, A.A.; Otis, R.; Dillon, R.P.; Borgonia, J.P.; McEnerney, B.W.; Hosemann, P.; Beese, A.M. Advances in additive manufacturing of metal-based functionally graded materials. *Int. Mater. Rev.* **2020**, *66*, 1–29. [CrossRef]

4. Lu, H.Z.; Liu, L.H.; Yang, C.; Luo, X.; Song, C.H.; Wang, Z.; Wang, J.; Su, Y.D.; Ding, Y.F.; Zhang, L.C.; et al. Simultaneous enhancement of mechanical and shape memory properties by heat-treatment homogenization of Ti_2Ni precipitates in TiNi shape memory alloy fabricated by selective laser melting. *J. Mater. Sci. Technol.* **2022**, *101*, 205–216. [CrossRef]
5. Saleh, B.; Jiang, J.; Fathi, R.; Al-hababi, T.; Xu, Q.; Wang, L.; Song, D.; Ma, A. 30 Years of functionally graded materials: An overview of manufacturing methods, Applications and Future Challenges. *Compos. Part B Eng.* **2020**, *201*, 108376. [CrossRef]
6. Chen, T.; Lu, H.Z.; Cai, W.S.; Liu, L.H.; Wang, Z.; Yang, C. Ultrastrong Ti–6Al–4V composite with hierarchical microstructure through two-step ball milling and pressureless sintering. *Scr. Mater.* **2023**, *236*, 115676. [CrossRef]
7. Li, P.; Cai, R.; Yang, G.; Wang, T.; Han, S.; Zhang, S.; Wang, W.; Meng, Q. Mechanically strong, stiff, and yet ductile $AlSi_7Mg$/graphene composites by laser metal deposition additive manufacturing. *Mater. Sci. Eng. A* **2021**, *823*, 141749. [CrossRef]
8. Sibisi, P.N.; Popoola, A.P.I.; Arthur, N.K.K.; Pityana, S.L. Review on direct metal laser deposition manufacturing technology for the Ti-6Al-4V alloy. *Int. J. Adv. Manuf. Technol.* **2020**, *107*, 1163–1178. [CrossRef]
9. Schwendner, K.I.; Banerjee, R.; Collins, P.C.; Brice, C.A.; Fraser, H.L.J.S.M. Direct laser deposition of alloys from elemental powder blends. *Scr. Mater.* **2001**, *45*, 1123–1129. [CrossRef]
10. Luo, X.; Song, T.; Gebert, A.; Neufeld, K.; Kaban, I.; Ma, H.; Cai, W.; Lu, H.; Li, D.; Li, N.; et al. Programming Crystallographic Orientation in Additive-Manufactured Beta-Type Titanium Alloy. *Adv. Sci.* **2023**, *10*, e2302884. [CrossRef]
11. Tan, C.; Sun, Q.; Xiao, L.; Zhao, Y.; Sun, J. Characterization of deformation in primary α phase and crack initiation and propagation of TC21 alloy using in-situ SEM experiments. *Mater. Sci. Eng. A* **2018**, *725*, 33–42. [CrossRef]
12. Li, W.; Yan, L.; Karnati, S.; Liou, F.; Newkirk, J.; Taminger, K.M.B.; Seufzer, W.J. Ti-Fe intermetallics analysis and control in joining titanium alloy and stainless steel by Laser Metal Deposition. *J. Mater. Process. Technol.* **2017**, *242*, 39–48. [CrossRef]
13. Abioye, T.E.; Farayibi, P.K.; Kinnel, P.; Clare, A.T. Functionally graded Ni-Ti microstructures synthesised in process by direct laser metal deposition. *Int. J. Adv. Manuf. Technol.* **2015**, *79*, 843–850. [CrossRef]
14. Boyer, R.R. An overview on the use of titanium in the aerospace industry. *Mater. Sci. Eng. A* **1996**, *213*, 103–114. [CrossRef]
15. Stephenson, P.L.; Haghdadi, N.; DeMott, R.; Liao, X.Z.; Ringer, S.P.; Primig, S. Effect of scanning strategy on variant selection in additively manufactured Ti-6Al-4V. *Addit. Manuf.* **2020**, *36*, 101581. [CrossRef]
16. Zhimin, H.; Yongqing, Z.; Weidong, Z.; Xiaonan, M.; Wenguang, L.; Pengsheng, Z. Effect of Heat Treatment on the Microstructure Development of TC21 Alloy. *Rare Met. Mater. Eng.* **2017**, *46*, 2087–2091. [CrossRef]
17. *GB/T 228.1-2010*; Metallic Materials—Tensile Testing—Part 1: Method of Test at Room Temperature. General Administration of Quality Supervision, Inspection and Quarantine of the People's Republic of China: Beijing, China, 2010.
18. Shi, R.; Dixit, V.; Fraser, H.L.; Wang, Y.J.A.M. Variant selection of grain boundary α by special prior β grain boundaries in titanium alloys. *Acta Mater.* **2014**, *75*, 156–166. [CrossRef]
19. Sallica-Leva, E.; Jardini, A.L.; Fogagnolo, J.B. Microstructure and mechanical behavior of porous Ti-6Al-4V parts obtained by selective laser melting. *J. Mech. Behav. Biomed. Mater.* **2013**, *26*, 98–108. [CrossRef] [PubMed]
20. Elshaer, R.N. Effect of Initial α-Phase Morphology on Microstructure, Mechanical Properties, and Work-Hardening Instability During Heat Treatment of TC21 Ti-Alloy. *Metallogr. Microstruct. Anal.* **2022**, *11*, 293–308. [CrossRef]
21. Lv, Z.; Ren, X.P.; Li, Z.H.; Lu, Z.M.; Gao, M.M. Effects of Two Different Cyclic Heat Treatments on Microstructure and Mechanical Properties of Ti-V Microalloyed Steel. *Mater. Res.* **2015**, *18*, 304–312. [CrossRef]
22. Vrancken, B.; Thijs, L.; Kruth, J.-P.; Van Humbeeck, J. Heat treatment of Ti_6Al_4V produced by Selective Laser Melting: Microstructure and mechanical properties. *J. Alloys Compd.* **2012**, *541*, 177–185. [CrossRef]
23. Kundu, S.; Sam, S.; Chatterjee, S. Interface microstructure and strength properties of Ti–6Al–4V and microduplex stainless steel diffusion bonded joints. *Mater. Des.* **2011**, *32*, 2997–3003. [CrossRef]
24. Han, J.-C.; Xiao, S.-L.; Tian, J.; Chen, Y.-Y.; Xu, L.-J.; Wang, X.-P.; Jia, Y.; Cao, S.-Z. Microstructure characterization and tensile properties of a Ni-containing TiAl-based alloy with heat treatment. *Rare Met.* **2015**, *35*, 26–34. [CrossRef]